COMPDYN 2015
5th ECCOMAS Thematic Conference on
Computational Methods in Structural Dynamics and Earthquake Engineering
M. Papadrakakis, V. Papadopoulos, V. Plevris (eds.)
Crete Island, Greece, 25–27 May 2015

MODEL-BASED JOINT INPUT-STATE ESTIMATION ON A THIN-WALLED CANTILEVER BEAM

Øyvind W. Petersen[1], Ole Øiseth[1] and Torodd S. Nord[2,3]

[1]Norwegian University of Science and Technology
7491 Trondheim, Norway
oyvind.w.petersen@ntnu.no, ole.oiseth@ntnu.no

[2] Centre for Sustainable Arctic Marine and Coastal Technology, Norwegian University of Science and Technology
7491 Trondheim, Norway
torodd.nord@ntnu.no

[3] The University Centre in Svalbard (UNIS)
Longyearbyen, Spitsbergen

Keywords: Force identification, response estimation, sensor network

Abstract. *In the field of structural dynamics, measuring external forces directly is often not feasible, whereas structural response data is far more accessible. Force identification is an inverse problem concerned with estimating forces using measured dynamic response. This paper presents a practical application of a joint input-state estimation algorithm. The algorithm gives minimum-variance unbiased estimates of states and input forces in a discrete-time linear system, where stochastic noise in the measurement data and model description are accommodated for. An experimental study of a thin-walled cantilever beam is presented to demonstrate joint input-state estimation. The finite element modelling is done in the software ABAQUS with shell elements. A modally reduced order model is created, containing 13 selected modes. We introduce the general approach of obtaining strain measurements in a modal format. A sensor network is designed from a discussion on optimal placement of accelerometers and strain gauges. It is also shown that the sensor network constitute a sufficient observational ensemble for estimation of states and forces. The studies demonstrate successful identification of forces generated by a simple mass-spring system. In addition, the strain is predicted at a location not co-located with the sensor network. The predicted strain agrees well with a reference strain measured at the same location. Lastly, we address some of the practical problems encountered and recommendations for further experiments.*

1 INTRODUCTION

1.1 Problem background

Force identification is a problem within structural dynamics concerned with estimation of external forces using measured dynamic response. Structural design and reliability assessment are areas where knowledge of model uncertainties of the forces to which the structure is exposed to is important. A better understanding of the true ambient forces could also be used to compare or update existing load models. In many cases, it is impractical to measure the forces directly, leading to the use of inverse identification methods. Herein, the inverse problem is solved to find the system inputs using the dynamic response together with an established system model. Often it is also desired to use the response data, sampled at a few locations, to estimate the complete structural response. If the true response is known, the information can be valuable for applications such as structural health monitoring, response to secondary installations or fatigue prediction.

In this paper we apply an established algorithm and show its feasibility for force identification and response estimation in a laboratory experiment on a thin-walled cantilever beam. Included is also a discussion on optimal placement of measurement sensors in light of recent advances on sensor networks.

1.2 Inverse force identification

Most practical cases of inverse identification are usually prone to ill-posedness since all state variables and initial conditions rarely are known [1]. The problem therefore has to be treated with special methods. Popular solution methods in the time domain feature Kalman filters [2, 3], occasionally in conjunction with least squares optimizers [4, 5]. We here present an application of the joint input-state estimation algorithm [6], which has a structure closely related to the Kalman filter. The algorithm was first introduced to structural dynamics by Lourens [7], who modified it to apply for modally reduced order models. The method has also has been verified experimentally by Lourens et al. [8] and Niu et al. [9]. Recently, it has also been applied by Nord et al. [10] to identify ice forces in a laboratory setting, giving input estimates in agreement with a reference solution by frequency domain deconvolution.

The framework for model-based force identification is often by means of finite element (FE) modelling and user-supplied parameters. Nord et al. [10] used a strain-displacement relation suitable for force identification using a model based on Timoshenko beam elements. We here aim to skip this step and let FE software directly provide all necessary parameters. The intent is to render an approach where the user does not have to supply strain-displacement relations manually.

2 FORCE IDENTIFICATION BY JOINT INPUT-STATE ESTIMATION

2.1 Stochastic state-space model

In applications of joint input-state estimation, the system is first transformed into state-space form. The basis is a time-invariant linear dynamic system with n_{DOF} degrees of freedom (DOFs) $\mathbf{u} \in \mathbb{R}^{\mathrm{n}_{DOF}}$:

$$\mathbf{M}\ddot{\mathbf{u}}(t) + \mathbf{C}\dot{\mathbf{u}}(t) + \mathbf{K}\mathbf{u}(t) = \mathbf{S}_{\mathbf{p}}\mathbf{p}(t) \tag{1}$$

Here, $\mathbf{M}$, $\mathbf{C}$ and $\mathbf{K}$ represents the mass, damping and stiffness matrix respectively, $\mathbf{S}_{\mathbf{p}} \in \mathbb{R}^{\mathrm{n}_{DOF} \times \mathrm{n}_p}$ is the force application matrix assigning the histories of the n_p external forces con-

tained in $\mathbf{p} \in \mathbb{R}^{\mathrm{n}_p}$ to the designated DOFs. When the damping is assumed proportional, the corresponding modally reduced order equation reads:

$$\ddot{\mathbf{z}}(t) + \mathbf{\Gamma}\dot{\mathbf{z}}(t) + \mathbf{\Omega}^2\mathbf{z}(t) = \mathbf{\Phi}^T\mathbf{S}_\mathbf{p}\mathbf{p}(t) \tag{2}$$

Here, $\mathbf{z} \in \mathbb{R}^{\mathrm{n}_m}$ is the vector with n_m selected modal coordinates and $\mathbf{\Phi} \in \mathbb{R}^{\mathrm{n}_{DOF} \times \mathrm{n}_m}$ is the corresponding mass-normalized mode shape matrix. $\mathbf{\Omega} \in \mathbb{R}^{\mathrm{n}_m \times \mathrm{n}_m}$ and $\mathbf{\Gamma} \in \mathbb{R}^{\mathrm{n}_m \times \mathrm{n}_m}$ are diagonal matrices collecting the natural frequencies ω_i and damping ratios ξ_i for every mode:

$$\mathbf{\Omega} = \mathrm{diag}(\omega_1, \ldots, \omega_{\mathrm{n}_m}), \quad \mathbf{\Gamma} = \mathrm{diag}(2\omega_1\xi_1, \ldots, 2\omega_{\mathrm{n}_m}\xi_{\mathrm{n}_m}) \tag{3}$$

The state-space transform is completed by rewriting Eq. 2 and defining the state vector $\mathbf{x} \in \mathbb{R}^{\mathrm{n}_s}$ ($\mathrm{n}_s = 2 \times \mathrm{n}_m$) and the system matrices $\mathbf{A}_c \in \mathbb{R}^{\mathrm{n}_s \times \mathrm{n}_s}$ and $\mathbf{B}_c \in \mathbb{R}^{\mathrm{n}_s \times \mathrm{n}_p}$ according to Eq. 5:

$$\dot{\mathbf{x}}(t) = \mathbf{A}_c\mathbf{x}(t) + \mathbf{B}_c\mathbf{p}(t) \tag{4}$$

$$\mathbf{x}(t) = \begin{pmatrix}\mathbf{z}(t)\\ \dot{\mathbf{z}}(t)\end{pmatrix}, \quad \mathbf{A}_c = \begin{bmatrix}\mathbf{0} & \mathbf{I}\\ -\mathbf{\Omega}^2 & -\mathbf{\Gamma}\end{bmatrix}, \quad \mathbf{B}_c = \begin{bmatrix}\mathbf{0}\\ \mathbf{\Phi}^T\mathbf{S}_p\end{bmatrix} \tag{5}$$

The discrete-time equivalent is found by introducing a sampling rate of $\frac{1}{\Delta t}$ together with a zero-order hold assumption on the force. An explicit solution to Eq. 4 then reads

$$\mathbf{x}_{k+1} = \mathbf{A}\mathbf{x}_k + \mathbf{B}\mathbf{p}_k \tag{6}$$

where $k \in \mathbb{N}$ is the time index and $t_k = k\Delta t$, $\mathbf{x}_k = \mathbf{x}(t_k)$, $\mathbf{p}_k = \mathbf{p}(t_k)$. The discrete system matrices $\mathbf{A} \in \mathbb{R}^{\mathrm{n}_s \times \mathrm{n}_s}$ and $\mathbf{B} \in \mathbb{R}^{\mathrm{n}_s \times \mathrm{n}_p}$ are defined as:

$$\mathbf{A} = e^{\mathbf{A}_c\Delta t}, \quad \mathbf{B} = (\mathbf{A} - \mathbf{I})\mathbf{A}_c^{-1}\mathbf{B}_c \tag{7}$$

The response measurements, n_d in total, are collected in the vector $\mathbf{y} \in \mathbb{R}^{\mathrm{n}_d}$ and related to the physical coordinates through selection matrices $\mathbf{S}_a, \mathbf{S}_v$ and $\mathbf{S}_d \in \mathbb{R}^{\mathrm{n}_d \times \mathrm{n}_{DOF}}$:

$$\mathbf{y}(t) = \mathbf{S}_a\ddot{\mathbf{u}}(t) + \mathbf{S}_v\dot{\mathbf{u}}(t) + \mathbf{S}_d\mathbf{u}(t) \tag{8}$$

Hence the measurements can be displacements, velocities and accelerations (or linear combinations of these). Rewritten on state-space form and subjected to the same discretization format as above, the measurement equation yields:

$$\mathbf{y}_k = \mathbf{G}\mathbf{x}_k + \mathbf{J}\mathbf{p}_k \tag{9}$$

Here $\mathbf{G} \in \mathbb{R}^{\mathrm{n}_d \times \mathrm{n}_s}$ and $\mathbf{J} \in \mathbb{R}^{\mathrm{n}_d \times \mathrm{n}_p}$ symbolizes the output influence matrix and direct transmission matrix, respectively:

$$\mathbf{G} = \begin{bmatrix}\mathbf{S}_d\mathbf{\Phi} - \mathbf{S}_a\mathbf{\Phi}\mathbf{\Omega}^2 & \mathbf{S}_v\mathbf{\Phi} - \mathbf{S}_a\mathbf{\Phi}\mathbf{\Gamma}\end{bmatrix}, \quad \mathbf{J} = \begin{bmatrix}\mathbf{S}_a\mathbf{\Phi}\mathbf{\Phi}^T\mathbf{S}_p\end{bmatrix} \tag{10}$$

Finally, the stochastic aspect is introduced by adding the model noise $\mathbf{w}_k \in \mathbb{R}^{\mathrm{n}_s}$ and the measurement noise $\mathbf{v}_k \in \mathbb{R}^{\mathrm{n}_d}$ to the state-space equations:

$$\mathbf{x}_{k+1} = \mathbf{A}\mathbf{x}_k + \mathbf{B}\mathbf{p}_k + \mathbf{w}_k \tag{11}$$

$$\mathbf{y}_k = \mathbf{G}\mathbf{x}_k + \mathbf{J}\mathbf{p}_k + \mathbf{v}_k \tag{12}$$

The former accounts for errors in the model description and the latter allow for inaccuracies in the measurement signals. Both are taken as zero mean white noise vectors and assumed mutally uncorrelated. The noise covariance, here assumed time invariant, is collected in the matrices $\mathbf{E}[\mathbf{w}_k\mathbf{w}_k^T] = \mathbf{Q}$ and $\mathbf{E}[\mathbf{v}_k\mathbf{v}_k^T] = \mathbf{R}$.

2.2 Joint input-state estimation

The joint input-estimation algorithm, originally developed by Gillijns [6], was further adapted to structural dynamics by Lourens et al. [8]. The algorithm is similar to the Kalman filter, except the true input is replaced by an optimal estimate [11]. It operates as follows:

- Estimate input forces by a minimum variance unbiased criteria (Eq. 13 - 16)
- Update state estimate with receiving measurement (Eq. 17 - 20)
- Estimate state ahead in time (Eq. 21 - 22)

$$\tilde{\mathbf{R}}_k = \mathbf{G}\mathbf{P}_{k|k-1}\mathbf{G}^T + \mathbf{R} \tag{13}$$
$$\mathbf{M}_k = (\mathbf{J}^T\tilde{\mathbf{R}}_k^{-1}\mathbf{J})^{-1}\mathbf{J}^T\tilde{\mathbf{R}}_k^{-1} \tag{14}$$
$$\hat{\mathbf{p}}_{k|k} = \mathbf{M}_k(\mathbf{y}_k - \mathbf{G}\hat{\mathbf{x}}_{k|k-1}) \tag{15}$$
$$\mathbf{P}_{\mathbf{p}[k|k]} = (\mathbf{J}^T\tilde{\mathbf{R}}_k^{-1}\mathbf{J})^{-1} \tag{16}$$

$$\mathbf{L}_k = \mathbf{P}_{k|k-1}\mathbf{G}^T\tilde{\mathbf{R}}_k^{-1} \tag{17}$$
$$\hat{\mathbf{x}}_{k|k} = \hat{\mathbf{x}}_{k|k-1} + \mathbf{L}_k(\mathbf{y}_k - \mathbf{G}\hat{\mathbf{x}}_{k|k-1} - \mathbf{J}\hat{\mathbf{p}}_{k|k}) \tag{18}$$
$$\mathbf{P}_{k|k} = \mathbf{P}_{k|k-1} - \mathbf{L}_k(\tilde{\mathbf{R}}_k - \mathbf{J}\mathbf{P}_{\mathbf{p}[k|k]}\mathbf{J}^T)\mathbf{L}_k^T \tag{19}$$
$$\mathbf{P}_{\mathbf{xp}[k|k]} = \mathbf{P}_{\mathbf{px}[k|k]}^T = -\mathbf{L}_k\mathbf{J}\mathbf{P}_{\mathbf{p}[k|k]} \tag{20}$$

$$\hat{\mathbf{x}}_{k+1|k} = \mathbf{A}\hat{\mathbf{x}}_{k|k} + \mathbf{B}\hat{\mathbf{p}}_{k|k} \tag{21}$$
$$\mathbf{P}_{k+1|k} = \begin{bmatrix}\mathbf{A} & \mathbf{B}\end{bmatrix}\begin{bmatrix}\mathbf{P}_{k|k} & \mathbf{P}_{\mathbf{xp}[k|k]} \\ \mathbf{P}_{\mathbf{px}[k|k]} & \mathbf{P}_{\mathbf{p}[k|k]}\end{bmatrix}\begin{bmatrix}\mathbf{A}^T \\ \mathbf{B}^T\end{bmatrix} + \mathbf{Q} \tag{22}$$

To initiate the estimation process, an initial state $\hat{\mathbf{x}}_{0|-1}$ with error covariance $\mathbf{P}_{0|-1}$ must be supplied. For an explanation of the covariance matrices (denoted $\mathbf{P}$ with varying subindex), refer to works by Gillijns and De Moor [11]. When the system and noise covariance matrices are time invariant, the filter often quickly reach a steady state. In this event the optimal weighing matrices for the state and the input, $\mathbf{L}_k$ and $\mathbf{M}_k$, remain unchanged in every step. The same holds for the error covariance.

2.3 Requirements for identification

Maes et al. [12] derived a set of criteria to be fulfilled in order to perform a successful identification of forces using joint input-state estimation in conjunction with a reduced order model. The design of a sensor network, i.e. determining types of measurements and sensor locations, plays a significant role in obtaining fair results. In addition to satisfying the criteria presented in Sec. 2.3.1 – 2.3.3, one must also recognize practical issues, such that the number of available sensors often is limited and the possible sensor locations restricted.

2.3.1 Observability

Observability concerns whether one is able to uniquely determine an initial state $\mathbf{x}_0$ from finite time series of known input forces and measurements. If this is true, the entire state history can be reconstructed from Eq. 6. In the case of the reduced order model, with none of the natural frequencies identical, the observability is fulfilled if and only if the matrix

$$(\mathbf{S}_d + \mathbf{S}_v + \mathbf{S}_a)\mathbf{\Phi} \tag{23}$$

does not contain any zero columns [12]. This can often intuitively be evaluated by interpreting the vectors of $\mathbf{\Phi}$ as modal configurations and the selection matrices as on-off buttons in each DOF. E.g. if a sensor is placed close to an inflection point of a mode, the mode will not be captured and and consequently its contribution to the total response cannot be judged. The observability criterion need only be fulfilled if state estimates are of interest, and not only the input.

2.3.2 Direct invertability

For system inversion without time delay, a direct invertability criterion must be met. $\mathbf{J}$, referred to as the direct transmission matrix, is important since it represents the direct influence from the input to the measurements, see Eq. 9. Direct invertability is fulfilled if and only if $\text{rank}(\mathbf{J}) = \text{rank}(\mathbf{S}_a\mathbf{\Phi}\mathbf{\Phi}^T\mathbf{S}_p) = \text{n}_p$ [12]. This is only ensured if the number of accelerometers is greater or equal to to n_p. In addition the forces must excite at least n_p modes distinguishable in the acceleration signals.

2.3.3 Stability

The stability in inversion of the state-space system depends on the transmission zeros λ_j [12], satisfying the relation:

$$\begin{bmatrix} \mathbf{A} - \lambda_j\mathbf{I} & \mathbf{B} \\ \mathbf{G} & \mathbf{J} \end{bmatrix} \begin{bmatrix} \mathbf{x}_0 \\ \mathbf{p}_0 \end{bmatrix} = \begin{bmatrix} \mathbf{0} \\ \mathbf{0} \end{bmatrix} \tag{24}$$

Under this condition, a force on the form $\mathbf{p}_k = \mathbf{p}_0\lambda_j^k$ will give a non-zero response while the observed measurements are identical to zero. Since the presence of such a force cannot be told, uniqueness in inversion is not achieved. Any $|\lambda_j| > 1$ is called an unstable transmission zero, however any $|\lambda_j| < 1$ is called stable since the undetectable force component converges towards zero when k increases. If $|\lambda_j| = 1$, marginal stability is obtained, signalling no data on static response is present. When strains or displacements are included to the sensor network, detection of static components corresponding to the 0 Hz frequency is restored. The matrix $\mathbf{J} - \mathbf{G}(\mathbf{A} - \mathbf{I})^{-1}\mathbf{B}$ should then be non-singular. Transmission zeros must be checked for all sensor configurations.

3 LABORATORY EXPERIMENT

3.1 Laboratory setup

Vibrations of a 3 m long cantilever beam are studied in the laboratory experiment. Notably, the extruded aluminium section has an unusual cross (+) shape, see Fig. 1. A 10 mm thick plate is welded to the beam end and bolted to a rigid wall. As shown in Fig. 1, washers separates the

end plate from the wall, allowing free movement in the end plate. The beam is free to bend both vertically and laterally. As a consequence of low torsional stiffness, torsional vibrations also composes an important component of motion. A brief list of the equipment used for acquiring data during the tests is listed in Table 1.

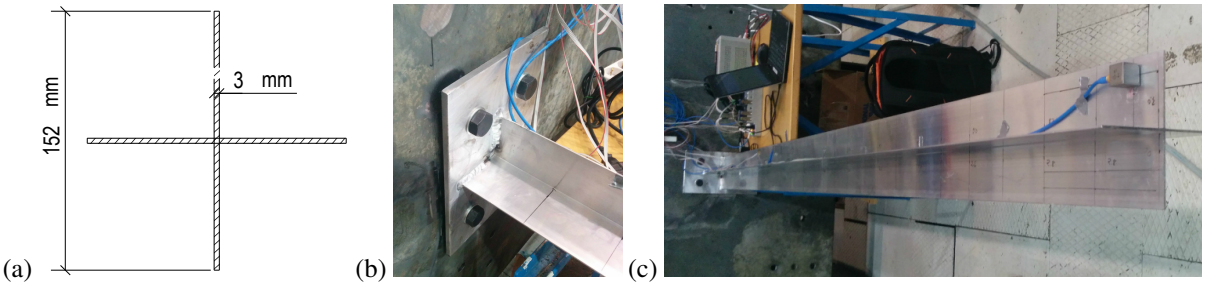

Figure 1: Left: cross section geometry; middle: bolted support and end plate-beam connection; right: beam mounted to wall (rotated).

Function	Model
Accelerometer	Kistler K-Beam 8395A, range $\pm$2g, sensitivity 2000 mV/g
Strain gauge	HBM 1-LV41-3/120 Ohm, Wheatstone quarter bridge
Accelerometer module	NI 9234
Strain module	NI 9235
Data acquisition system	NI cDAQ-9178

Table 1: List of equipment used for acquiring measurement data.

3.2 Finite element model

A FE model of the thin-walled section was created using 8-node quadrilateral shell elements (S8R) in the software ABAQUS. Translational DOFs in the end plate at the location of the bolts were pinned. The mesh was generated using an average element width of 20 mm. It is evident that the support and its rotational stiffness would be more difficult to model using beam elements. In addition, conventional beam elements could have problems describing the torsional behaviour of the section, advocating the choice of shell elements. Mode shapes, natural frequencies as well as the modal strain parameter $\mathbf{S}_d\mathbf{\Phi}$ were extracted from the FE model. Exact shape functions of the element are therefore not explicitly needed by the user to relate strains and displacements. The reduced order model is here comprised of the 13 modes with lowest natural frequencies, which of 6 are bending modes and 7 are torsional, see Table 2. The damping ratio is taken as 0.3% for all modes. Some of the modes relevant for vertical eccentric loading is displayed in Fig. 2.

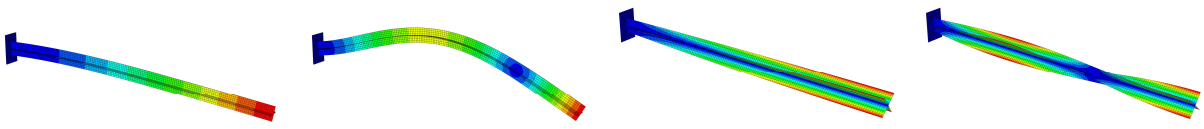

Figure 2: Mode 2, 7 (vertical bending), 3 and 4 (torsion).

n	f_n [Hz]	Type
1	7.8	Lateral bending
2	9.2	Vertical bending
3	10.5	Torsion
4	31.4	Torsion
5	51.7	Lateral bending
6	52.5	Torsion
7	57.3	Vertical bending
8	73.8	Torsion
9	95.4	Torsion
10	117.4	Torsion
11	139.9	Torsion
12	146.0	Lateral bending
13	156.2	Vertical bending

Table 2: Natural frequencies of FE-model.

3.3 Optimal sensor placement

In this section we study positioning of sensors in relation to the criteria described in Sec. 2.3. Two triaxial accelerometers and three uniaxial strain gauges are disposable for the sensor network. First, the accelerometer locations are determined. The objective is to ensure the direct transmission matrix $\mathbf{J} = \mathbf{S}_a\mathbf{\Phi}\mathbf{\Phi}^T\mathbf{S}_p$ has full rank. $\mathbf{S}_p$ is determined by setting the force action point eccentrically at the cantilever end, 40 mm from the centroid, see Fig. 3. It is seen from the quantity $\mathbf{\Phi}^T\mathbf{S}_p$ in Fig. 4 that a vertical force component (316y) induces vertical bending and torsion in the beam, while the lateral component (316z) excites lateral bending modes only.

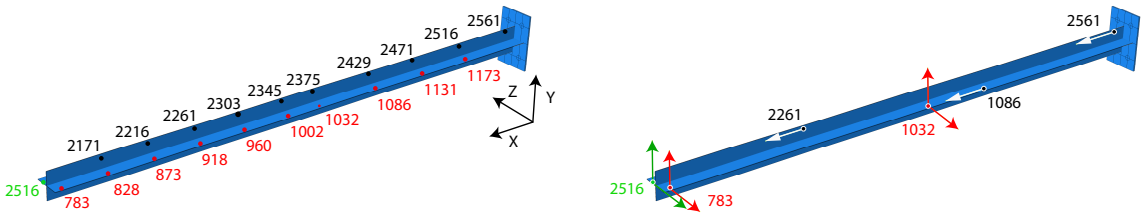

Figure 3: Geometry and sensors: accelerometers (red), strain gauges (black) and force (green): Left: possible sensor nodal positions; right: final sensor network denoted with measuring directions.

In the following, accelerometer locations approximately 60 mm from the centroid as shown in Fig. 3 are considered. $\mathbf{S}_a\mathbf{\Phi}$, interpreted the modal projections on accelerometer locations, are sought to be maximized for the modes to have good influence on the sensors. In Fig. 4 we promptly identify the cantilever tip location (783y) to be suitable for capturing bending (modes 2, 7, 13) as well as torsion (modes 3, 4, 6, 8-11). For the second accelerometer, 1032y seems as a feasible choice with good modal influence for all modes except lateral bending. For reasons of symmetry in geometry, similar results are obtained when repeating the procedure for lateral accelerations in the same nodes, but are left out here. Acceleration data for the x-direction is discarded since none of the incluced modes exhibit axial motion. When $\mathbf{S}_a$ is determined from accelerometers measuring in node 783 and 1032 in both y-direction and z-direction, $\text{rank}(\mathbf{J}) = \text{n}_p = 2$ and direct invertability is ensured.

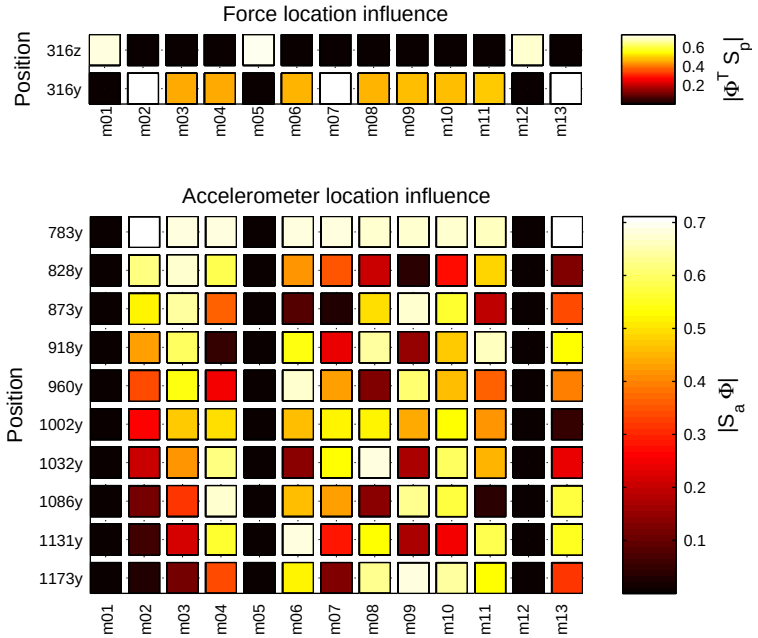

Figure 4: Top: Force influence for lateral (z) and vertical (y) component. Bottom: Accelerometer influence in vertical direction (y) for a variety of locations.

No unstable transmission zeros exist for this network of accelerometers. However, the system is marginally stable without measurement data sensitive to static loading. In a similar manner as above, we look at possible strain gauge locations through $\mathbf{S}_d\mathbf{\Phi}$ in Fig. 5 with the goal to maximize modal influence. For the lowest vertical bending mode (m02) the influence is limited for all positions, but highest close to the support (2561x, value 0.014). This location is therefore included. 2261x appear as the best choice for a second sensor. Again, similar results are obtained when considering the location of a third strain to capture lateral bending modes. For this specific problem, shear strain could also be measured to increase the influence from torsion modes. The total network ($\mathrm{n}_d = 7$) including the third strain gauge is shown in Fig. 3. The marginal transmission zeros are now eliminated for this sensor configuration. We further check this from $\mathbf{J} - \mathbf{G}(\mathbf{A} - \mathbf{I})^{-1}\mathbf{B}$, whose singular values are 0.189×10^{-5} and 0.314×10^{-5}, concluding the matrix has full rank.

For the observability criteria, the single accelerometer at the end suffices since this is a non-zero point for all modes. The states should therefore be estimated adequately with the entire sensor network. We readily confirm $(\mathbf{S}_d + \mathbf{S}_a)\mathbf{\Phi}$ has no zero columns.

3.4 Data acquisition and noise parameters

The load, applied eccentrically at the free end of the beam, was induced by attaching a spring supported mass ($k \approx 180$ N/m, $m = 0.78$ kg). The spring was given an initial displacement, and upon release the free vibrations of the combined beam spring-mass system were sampled at a rate of 2048 Hz. In addition to the described sensor network, the strain in node 2429 (cf. Fig 3) was measured to later serve as a reference in response prediction. The acceleration data series was detrended and low-pass filtered (6. order Butterworth filter, cutoff frequency 350 Hz) to hinder the filter receiving data in the frequency range above the includes modes, which could lead to difficulties when compensating for unexpected behaviour. The same was done for the

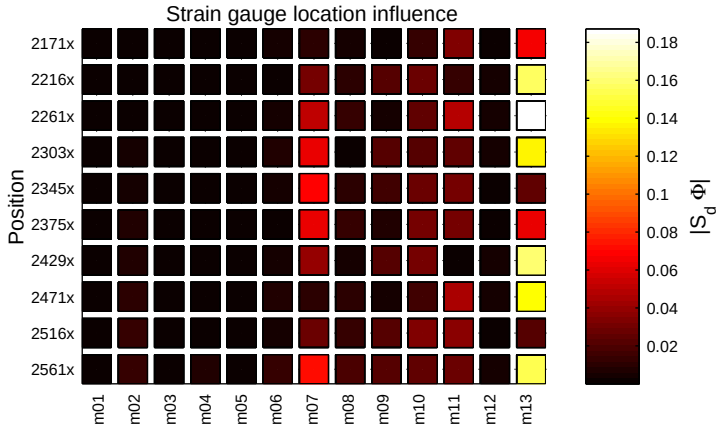

Figure 5: Influence for strain gauges measuring in beam longitudinal direction (x).

strain data, but with a cutoff frequency of 50 Hz since the data was severely contaminated with colored noise from the AC power supply.

When determining the noise covariance matrix ($\mathbf{R}$), not only the latent white noise in the sensor signals must be included, but also disturbances originating from second order effects, deviation in sensor locations and sensor accuracy in the prevailing frequency range. In view of this, the noise magnitude can be challenging to quantify. In addition, the correlation is usually unknown and is therefore often assumed as zero. Similar difficulties are encountered when deciding the model noise ($\mathbf{Q}$). Model errors in natural frequencies and damping ratios, system non-linearities, and the accuracy of the discretization in Eq. 6 will contribute to the noise. A common solution is to choose the noise magnitudes as a small percentage of the variables they represent [7]. The diagonal elements of $\mathbf{R}$ corresponding to accelerations were set to 10^{-4} and for strains to 10^{-14}. Likewise for $\mathbf{Q}$, diagonal elements were fixed as 10^{-12} and 10^{-10} for the modal displacements and velocities, respectively.

4 RESULTS AND DISCUSSION

4.1 Force identification

The forces identified with the joint input-state estimator are shown in Fig. 6. The total force magnitude is approximately 6 N, corresponding to 30 mm elongation of the spring. The frequency content in Fig. 7 shows the forces are dominant at 2.4 Hz, a feature of the spring-mass. Since the spring elongation also depends on the cantilever deflection at the force action point, a peak is seen at 9 Hz for the y-component. This originates from the lowest vertical bending and torsion mode, which for the real structure has very close natural frequencies. Although there are some discrepancy between the modelled and true natural frequencies, the filter fairly adjusts the results in favor of the true behaviour. The same is observed at 9 Hz (torsion) for the lateral component.

However, the result should be interpreted with caution. The results are dependent on the prescribed model noise. In particular, spurious compensating forces can occur if the system model differs too much from the real behaviour. Similarly, the measurement noise covariance affects the weighting between acceleration signals, dominant at the natural frequencies, and strain signals, dominant at the forcing frequency.

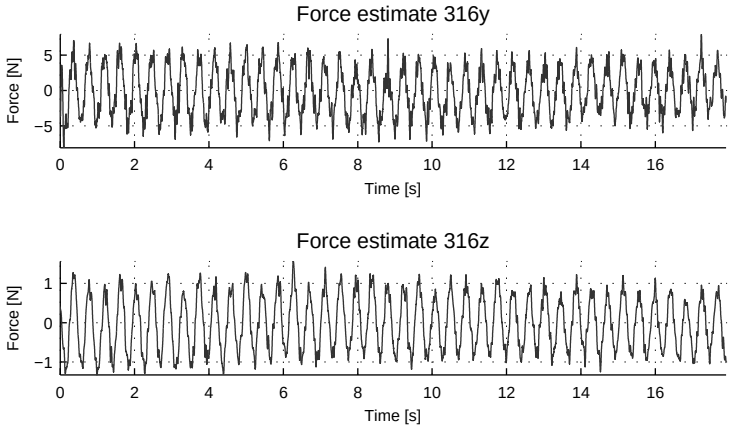

Figure 6: Time series for the identified vertical (316y) and lateral (316z) force component.

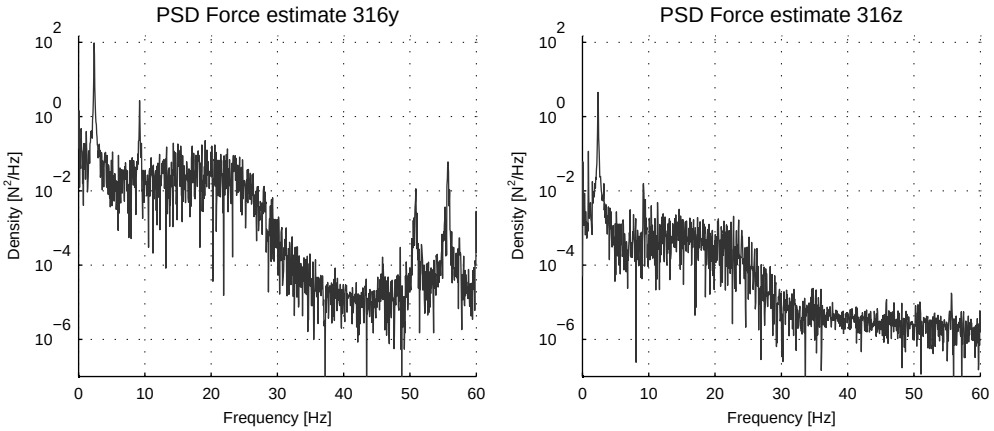

Figure 7: Power spectral density of the vertical (316y) and lateral (316z) force component.

4.2 Response estimate

To check the quality of the response estimate, the reference strain measured in node 2429 (cf. Fig 3) is studied. A prediction of the strain in the same node, collected in $\hat{\mathbf{y}}_k$, can be generated from the set of state estimates, $\hat{\mathbf{x}}$, obtained simultaneously with the force estimates. Furthermore, new selection matrices ($\mathbf{S}_a = \mathbf{S}_v = \mathbf{0}$, $\mathbf{S}_d \neq \mathbf{0}$) are created and $\hat{\mathbf{x}}$ is inserted in Eq. 9, yielding:

$$\hat{\mathbf{y}}_k = \begin{bmatrix} \mathbf{S}_d\boldsymbol{\Phi} & \mathbf{0} \end{bmatrix} \hat{\mathbf{x}}_k \tag{25}$$

A comparison of the predicted and measured strain is plotted in Fig. 8. The frequency and amplitude coincides remarkably well. The result suggests the states are estimated accurately.

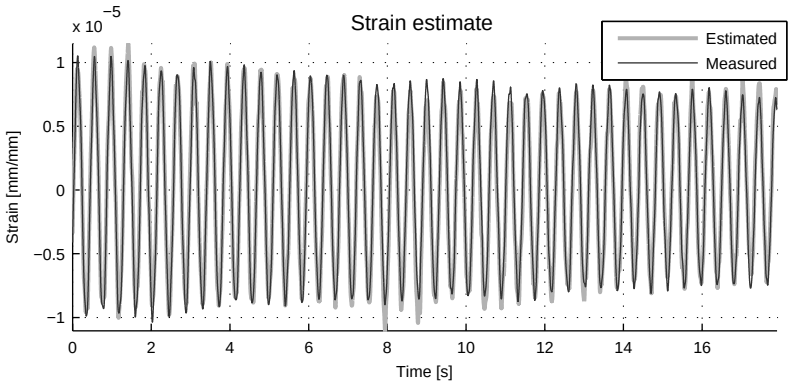

Figure 8: Comparison of predicted and measured strain in node 2429.

5 CONCLUDING REMARKS

The forces on a structure that cannot be measured directly can instead found by using measured dynamic response. We have in this paper applied a joint input-state estimation algorithm to estimate the forces and response for a cantilever beam. The FE model was established using shell elements, which for the thin-walled section has been shown as a viable approach. The designed sensor network, consisting of accelerometers and strain gauges, meets the criteria for joint input-state estimation with reduced order models. The force estimates obtained by the algorithm are reasonable. In addition the response at an unmeasured point of the structure has been successfully predicted.

To properly verify the identified force is correct, the true force can be measured directly to serve as a reference solution. In addition, system identification techniques could be applied to make the model a closer resemblance of the real structure. This would be even more important if identification of a more broad banded force were performed. A hammer impact, for example, would also involve the higher modes to a larger extent, which could give interesting results. For the presented study, the accelerometers had a measuring range of only $\pm$2g, meaning the motion had to be limited. As a consequence, very low bending strains are observed, causing a critical low signal to noise ratio. An other problem encountered the tests is the high flexibility of the section, which for even moderate movements gives rise to second order effects (i.e. displaced geometry axes), affecting the sensor signals. A set of simulated measurement data can also be generated if the force are measured directly. A comparison of the real and simulated data could then be used to better quantify the measurement noise.

REFERENCES

[1] T. Uhl. The inverse identification problem and its technical application. *Archive of Applied Mechanics*, 77(5):325–337, 2007.

[2] E.-M. Lourens, E. Reynders, G. De Roeck, G. Degrande, and G. Lombaert. An augmented Kalman filter for force identification in structural dynamics. *Mechanical Systems and Signal Processing*, 27:446–460, 2012.

[3] J.-S. Hwang, S.-G. Lee, P. Ji-hoon, and Y. Eun-Jong. Force identification from structural responses using Kalman filter. In *Materials Forum*, volume 33, 2009.

[4] C. K. Ma, J. M. Chang, and D. C. Lin. Input forces estimation of beam structures by an inverse method. *Journal of sound and vibration*, 259(2):387–407, 2003.

[5] J.-J. Liu, C.-K. Ma, I.-C. Kung, and D.-C. Lin. Input force estimation of a cantilever plate by using a system identification technique. *Computer Methods in Applied Mechanics and Engineering*, 190(11):1309–1322, 2000.

[6] S. Gillijns. *Kalman Filtering Techniques for System Inversion and Data Assimilation*. PhD thesis, Katholieke Universiteit Leuven - Faculty of Engineering Technology, Leuven (Belgium), 2007.

[7] E.-M. Lourens. *Force identification in structural dynamics*. PhD thesis, Katholieke Universiteit Leuven - Faculty of Engineering, Leuven (Belgium), 2012.

[8] E.-M. Lourens, C. Papadimitriou, S. Gillijns, E. Reynders, G. De Roeck, and G. Lombaert. Joint input-response estimation for structural systems based on reduced-order models and vibration data from a limited number of sensors. *Mechanical Systems and Signal Processing*, 29:310–327, 2012.

[9] Y. Niu, M. Klinkov, and C.-P. Fritzen. Online force reconstruction using an unknown-input Kalman filter approach. In *Proceedings of the 8th International Conference on Structural Dynamics,*, pages 2569–2576, EURODYN 2011.

[10] T. S. Nord, E.-M. Lourens, O. Øiseth, and A. Metrikine. Model-based force and state estimation in experimental ice-induced vibrations by means of Kalman filtering. *Cold Regions Science and Technology*, 111:13–26, 2015.

[11] S. Gillijns and B. De Moor. Unbiased minimum-variance input and state estimation for linear discrete-time systems with direct feedthrough. *Automatica*, 43(5):934–937, 2007.

[12] K. Maes, E.-M. Lourens, K. Van Nimmen, E. Reynders, G. De Roeck, and G. Lombaert. Design of sensor networks for instantaneous inversion of modally reduced order models in structural dynamics. *Mechanical Systems and Signal Processing*, 2014.